The Probability of the moiré effect in parallax-barrier and lenticular autostereoscopic 3D displays

Abstract: Angles of the moiré patterns are measured experimentally. Two kinds of clustering were observed in the parameter space. In rational cells (LCD pixels), the moiré patterns appear at a few discrete angles. The experimental probability of the moiré effect is estimated as a function of angle; a theoretical function (node spacing) is based on the distance between nodes. The connection between the probability of the moiré effect, the Thomae's function, and other functions is found. The proposed approach can be used to minimize the moiré effect in visual displays, especially in autostereoscopic 3D displays.

Keywords:moiré effect, moiré patterns, moiré minimization, moiré probability, autostereoscopic displays, moiré statistics

---

1. Introduction

The moiré effect is a visual opticalphenomenoninsuperposed transparent repeated structures [1]-[3]. In visual displays,the moiré effect may create a meaningless visual image of bands (a visual noise). The layers are typical for autostereoscopic three-dimensional displays [4], [5];one layer usually is the pixelated LCD screen, and another is a lenticular or barrier plate; the ratio of the periods of layers is commonly integer[6]. The layered structure with the integer ratio gives riseto noticeable moiré patternsthat reduce a displayed image's visual contrast. It is essential to reduce (minimize) the moiré effect to minimize the moiré effect in visual displays, especially in autostereoscopic 3D displays. Therefore, the elimination or at least reduction (minimization) of the moiré effect is a significant issue in improving the visual quality of displays, especially the autostereoscopic three-dimensional multiview displays and integral imaging displays[2], [7],[8].

Characteristics of the patterns may have local minima and maxima across an angular range.The moiré patterns may have too smalland unrecognizable amplitude at some angles.At other angles, the pattern can be easily detected.We consider the period of the moiré patterns as a function of the rotation angle.The maxima of the amplitude correspond to the strongest patterns, and the minima relate to the weakest patterns or their absence.The "moiré angles" are the angles of the local maxima of the amplitude.According to the visibility assumption [9], the longerthe period of the patterns,the higher the visibility.

The experiments have uncovered a novel relationship between the angle variation and the moiré patterns.This variation not only changes the period and orientation of the patterns [10] but also affects their visibility.When the period of the moiré patterns is near a local maximum, the patterns are most visible (among neighboring angles), based on the visibility assumption [9]. An example of the experimental moiré period as a function of angle is shown in Fig. 1 for a display device with a period of pixels of 0.266 mm and a lenticular plate of 50 lpi (period 0.508 mm). In the experiment, we did not observe moiré patterns with a period shorter than 0.8 mm, similar to [11].

Comment [A1]: What is node spacing? What is a node? Clarify in the main body!

Comment [A2]: Which has minima o maxima? Is it the characteristics o the pattern. The sentence is vague.

Comment [A3]: What is meant by angle or angular angle? Is it the angle of illumination or the observer? Please clarify.

Comment [A4]: Same as above.

Comment [A5]: What is the meaning of Moire pattern? Is it the shadow or the actual pattern on the mask? Please clarify.

Comment [A6]: What is meant by strongest or weakest pattern? Are we talking about a whole pattern (dark and transparent lines) or talking about an area in a pattern. How opaque and transparent pattern be strong or weak? Or you mean the illumination. This is confusing; it needs clarification.

Comment [A7]: You need to illustration explain the meaning of this paragraph.

Comment [A8]: Relationships are normally between parameters. How can we get a relationship between a pattern and a variation of an angle. Is it between one of the pattern parameters and the value of the angle? Authors need to precise.

Comment [A9]: Although this statement is referenced. It needs to be made clear. Explain orientation of pattern.

Comment [A10]: Statements are referenced, but must be clear to the reader. This is a book chapter and needs to be self explanatory.

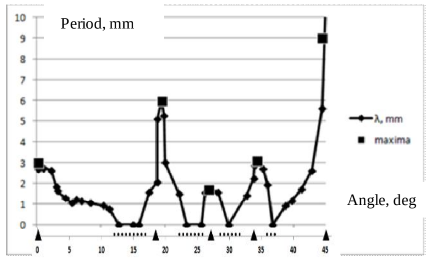

Fig. 1. The experimental graph of the moiré period vs. twist angle in a typical LCD display. Reproduced from [14].

Comment [A11]: Define the twist angle in the text with illustration, preferable to be 3D.

The above experimental graph of the moiré period has several maxima. It is known [12] that the amplitude and the period of the moiré patterns in the twisted gratings reach the maxima at the same angle. For instance, there are several local maxima in the experimental data [13]: two at the edges of the domain and three in the middle.

There are five maxima of different heights and widths in Fig. 1; however, this is just a particular example, not a general case; in another device, a similar graph may look differently; for instance, the number of maxima and the relative height of the peaks can be different. Typically, the peaks at 0° and 45° at the edges of the domain are the widest, and in the case shown in Fig. 1, the moiré patterns were detected within the angular regions at approx. ±16° and ±6° around 0° and 45°, resp. Three other peaks are essentially narrower (their half-width is between ±1° and ±2.5°). This experiment detected No moiré patterns with a period shorter than 0.8 mm.

The statistics is not commonly used to study the moiré phenomenon, but it has practical applications. The probability function isapplied to theelimination of the moiré patterns[15]. The probability of the time-averaged moiré fringes is considered in [16]. The probability was mentioned in [17] for the moiré superstructures. A statistics-based moiré method was applied to the characterization of the moiré structuresin [18].

In the current Chapter, we consider the moiré angles (the local maxima of the moiré period)as in the example shown in Fig. 1, characterize them in statistical terms, and define a theoretical and experimental probability of the moiré effect in the square grid as a function of the twist angle.The study [19] presents the moiré angles in autostereoscopic LCDs with barrier plates and analyzes their distribution in the parameter space. Mainly, the moiré occurrences in double-layer devices (with lenticular and barrier plates) are analyzed from the statistical point of view and the experimental probability function is built. The experimental probability function [13] is based on the experiments with the barrier displays, while the function for the LCD displays with lenticular plate was presented in [20].We also define a theoretical probability function of the moiré effect in the square grid as a function of the twist angle and introduce a combined function for both types of the autostereoscopic displays.

We compare the experimental and theoretical data in the autostereoscopic barrier and lenticulardisplays and build the composite function.We also build the theoretical function and compare it with related functions.

The current Chapter is based on the research papers [19], [21],and partially [14].The Chapter includes the experimental results for several display devices.We have arranged the Chapter as follows. In Section 2, we present the theory, including the rational angles and the orientation of the moiré patterns at the moiré angles;we also describe a simple technique to detect the maximal period of the moiré patterns based on their angle.Section 3 describes the experimental resultswith the parallax-barrier and lenticular displays, including different aspect ratios and the experimental probability. Section 4 presents the probability function and compares the experimental results with the theory. The related functions (theoretical and experimental) are presented in Section 5. Then, Section 6 presents a brief discussion, and Section 7 concludes the Chapter.

2. Theory

2.1. Rational Angles on Square Grid

The angles can be characterized in a variety of ways. We call the angle, whose tangent is a rational number, a rational angle, in the same way as [22],

$$\varphi_{mn} = \arctan \frac{m}{n} \qquad (1)$$

where m, n are non-negative integer numbers (0, 1, 2, …), typically ≤ 4. The rational angles satisfying Eq. (1) can be characterized by pairs of non-negative integer numbers (m, n).

The scientific research [12] has experimentally confirmed a significant finding that the moiré angles coincide with the maxima of the period. This has aspecial significance. In Fig. 1, triangles on the abscissa indicate the rational angles; in this preliminary experiment, m and $n$were not higher than 3.

In digital displays, the aspect ratio of pixels istypically a rational number;this plays a vital role in the appearance of moiré patterns at the rational angles, as Ref. [19] confirms. In LCD, for instance, the aspect ratio of pixels is rational because of their typical arrangement in a square grid.

Fig. 2 illustrates the rational angles on the square grid. The circles indicate the intersections of the nodes of the grid with the rays from the origin; the numbers near the edges of the graph are the tangents of slant angles.The non-rational (i.e., irrational) angles do not satisfy Eq. (1); they lie somewhere between the rational ones.

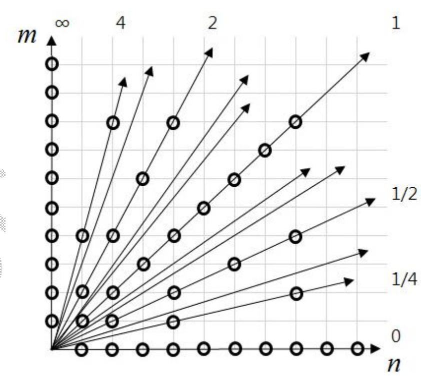

Fig. 2. Slope of rays and the grid. Reprinted with permission from [21]. © The Optical Society.

The rays with the rational tangentsm/nrepeatedly cross the nodes (jm, jn), where $j$is an integer.In contrast, the non-rational rays never cross a node (and theirtangent cannot be represented as a ratio of the integer numbers).

2.2. SpacingFunction

A numerical characteristic of a ray could be thedistance between nodes along rays in the square grid (i.e., spacing). For example, the ray m = 0, n = 1 has the unit distance between the nodes, while the ray m = n = 1 has the distance of$\sqrt{2}$.The distance between the nodes (spacing) differs for the rays at different angles. The number of crossed nodes per length unit defines the spacing.We can calculate it based on the first of repeated intersection points (corresponding to the coprime numbers *m* and *n*).

We define the spacing asa reciprocal distance between the nodes

$$D(x) = \begin{cases} \dfrac{1}{\sqrt{m^2 + n^2}} & \text{for rational angles } (x = m/n) \\ 0 & \text{for non-rational angles} \end{cases} \qquad (2)$$

Figure 3 shows the spacing as a function of the angle, the theoretical function describing the angles concerning the square grid nodes. The irrational rays never cross a node. Therefore, the distance between the nodes (spacing) for such rays is infinite.

Comment [A12]: What do you mean by spacing? Spacing is between points. Clarify!

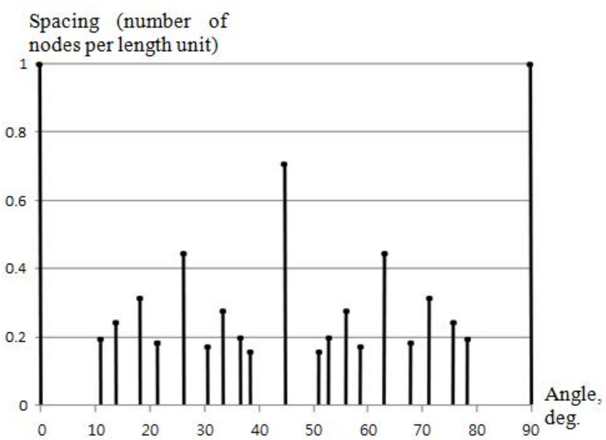

Fig. 3. Calculated spacing of nodes (theoretical function) for *m*, *n* ≤ 5. Reprinted with permission from [21]. © The Optical Society.

2.3. Moiré Angles

We refer to the angle with the local maximum of the period of the moiré patterns as the moiré angle. Thus, at the moiré angles, the period reaches a local maximum, and the moiré patterns are parallel to the axis of the rotated grating.We can explain this feature in the spectral domain. The wavevector of a moiré pattern is the ray from the origin to the spectral component under consideration. The change of the angle α_1 between the grating and the plate (see Fig. 4) makes the rotation of the spectral component around the center*A*along the circular arc *l*. This rotation can be treated as the movement of the component along a particular trajectory (which, in this case, is the circular arc *l* in Fig. 4). In this movement, the moiré period changes together with the orientation of the patterns (the angle α_2), as described in [10].

Comment [A13]: How grating is rotated. Illustration is needed to explain this rotation. Fig. 4 may not give the first time reader a clear picture about the rotation. For example, is the grating rotation horizontal, or vertical, or free rotation? From Fig 4, if point A moves, we still have $\alpha_1 = \alpha_2$. Therefore, I suggest that an illustration (3D)showing how the grating is rotated with respect to the projection plan.

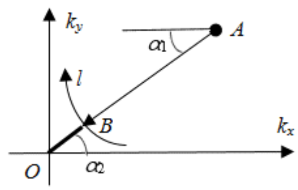

Fig. 4. The maximal moiré period (spectral domain). Reprinted with permission from [21]. © The Optical Society.

While the trajectory *l*passes the neighborhood of the origin, the wavenumber closes the minimum.Thus, the period reaches a maximum at point *B*, where the trajectory *l*crosses the line*OA*connecting the origin *O*and the center*A* of the trajectory. Here, the angles α_1 and α_2 are equal;therefore,the moiré patterns are parallel to the grating axis.

Regarding the moiré effect, the rational angles have additional significance since it was experimentally proven [19] that the moiré effect happens more or less frequentlyat different angles.The moiré effect at different angles occurs with varying frequency. In displays with rational cells, moiré angles can be classified into two major categories, “often” and “rare” angles. This classification is particularly useful in understanding the occurrence of moiré patterns in lenticular displays at the rational angles, as stated in [19]. Therefore, in this Chapter, we will consider the moiré effect in the periodic layers of the lenticular and barrier 3D displays with the rational cells, focusing on the classification and occurrence in terms of probability.

3. Experiments

In order to find the moiré angles φ experimentally, we performed experiments with the printed samples (using a desktop laser printer) and with the LCD panels.Therotating (twisted) parallax barrier plates and lenticular plates were applied to the panelsand samples in these experiments.The observation distance was 50 cm, and the range of the geometric parameters ρ and σ(the ratio of periods and the aspect ratio) was between 0.18 and 3. The range of the running angle α selected based on the symmetry; it was 0 - 90° in general, but 0 - 45° for square cells. These parameters correspond to a typical stereoscopic display or a multiview display with subpixels. Indeed, the appearance of the moiré patterns in each case depends on the specific values of the parametersα, ρ, and σ. We took most care about the period (because the direction of the patterns at the moiré angle is known, as described in Sec. 2.3). In total, 5 LCD devices (with a fixed σ) and various printed samples (within a wide range of σ) were combined withthree barrier plates in various combinations.

A continuous angular range was tested for the moiré effect in LCD panels (square cells) and printed rectangular grids (rectangular cells of various aspect ratios) printed on paper and transparencies. In these experiments, we took the panels and samples and superimposed them withthe barrier plates.

3.1. Experimental Equipment

The periods of the barrier plates were 0.44 mm, 0.45 mm, and 0.57 mm, while the periods of printed samples varied between 0.24 mm and 2.4 mm; the aspect ratio of these samples was in a range between 0.33 and 3. We made the experiment with 27 values of σ and 2 values of ρ, which means 54 particular tests. Experiments with lenticular displays were made with 8 displays (the screen size from 7 in. to 24 in., where 1 in. = 2.54 cm); the pixel pitch from 0.06 mm to 0.27 mm) and 5 lenticular plates (15 – 75 lpi, i.e., the period from 0.39 mm to 1.69 mm) in various, arbitrary combinations. Tables 1 and 2 list the lenticular plates and LCD panels.

Comment [A14]: Define kx and ky. Are these wavevectors as in quantum physics? Or they refer to something else?

Figure caption needs to be more informative.

Comment [A15]: This needs illustration to visualize the rotation and the relative position of every plate.

Comment [A16]: This needs illustration to visualize the rotation and the relative position of every plate. Show all parameters and the position of the LCD plate. Make it 3D.

Comment [A17]: 3D illustration. Either new one or refer to previous ones.

Table 1. Lenticular plates were used in experiments.

No	Lines per inch, lpi	Pitch, mm
1	12	2.1
2	15	1.7
3	25	1.02
4	40	0.64
5	50	0.51
6	75	0.34

Table 2. Display devices used in experiments.

No	Alphabetic index	Model	Pixel pitch, mm	Screen diagonal, in.	Screen diagonal, cm	Resolution, pixels
1	A	BTC Zeus 7000	0.27	24	61	1920 x 1200
2	B	Samsung NT-N310	0.214	10	25.4	1024 x 600
3	C	Samsung Sens Q35	0.204	12.1	30.7	1280 x 800
4	D	First FS-i07BS	0.1905	7	7	800 x 480
5	E	Crossover 3020MDP	0.2505	30	17.8	2560 x 1600
6	F	LG Flatron WX2353	0.266	23	58.4	1920 x 1080
7	-	HP Pavilion dv6	0.18	15.6	39.6	1920 x 1080
8	-	Samsung Galaxy-5	0.059	5.1	13	1080x1920

In experiments, a static image was displayed:the black rectangular grid on the white background for printed images and the grid of pixels themselves for LCD panels with auniform white screen). The angle α between the static image (printed grid or panel) and the barrier plate was gradually changed from 0 to 90°. As the plate rotates, the angles where the moiré effect occursaredetermined and recorded. This way, the moiré anglesφ were detected.

Comment [A18]: Where is this black rectangular grid. Show a drawing for it.

We performed two experiments with the barriers: 1) an arbitrary aspect ratio of grid cells (in printed samples), including the rational aspect ratio,

$$\sigma_{kl} = \frac{k}{l} \quad (k,\, l \text{ integers}) \tag{3}$$

and 2)square pixels (in LCD panels). With the printed samples, the aspect ratio σ changed from 0.17 to 3.0,and the size ratio ρ varied between 0.18 and 0.72.In LCD experiments(σ = 1), ρranged between 1.62and 3.0. In the lenticular experiments, the pixel pitch of LCDs varied from 0.1905 mm to 0.27 mm, the pitch of lenticular plates was between 12 and 40 lenticular lenses per inch (lpi), i.e., from 0.64 mm to 2.17 mm. Consequently, the ratio ρ varied between 2.5 and 8.89.

It can be said in advance that the moiré anglesφ= 0 and 90° were observed in all displays with any combination of parameters σ and ρ between 0.18 and 3.

3.2. Experimental Moiré Angles inBarrierDisplays

The visual observation was made from 50 cm away, and the photographs were taken from that distance. Fig. 5 shows examples of the photographed moiré patterns whenthe angle between the gratings is 0°.Examples of the observed moirépatternsin printed samplesat other angles are shown in Fig. 6.

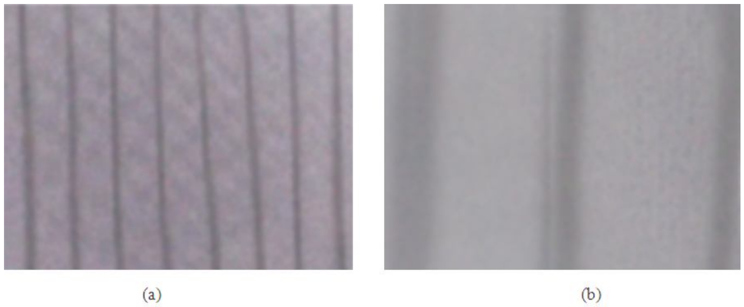

Fig. 5. Examples of moiré patterns in printed samples. The aspect ratio is 0.33 in (a) and 0.58 in (b); the ratio of periods is 0.72 and 0.44, resp.Reproduced with permission from [21]. © The Optical Society.

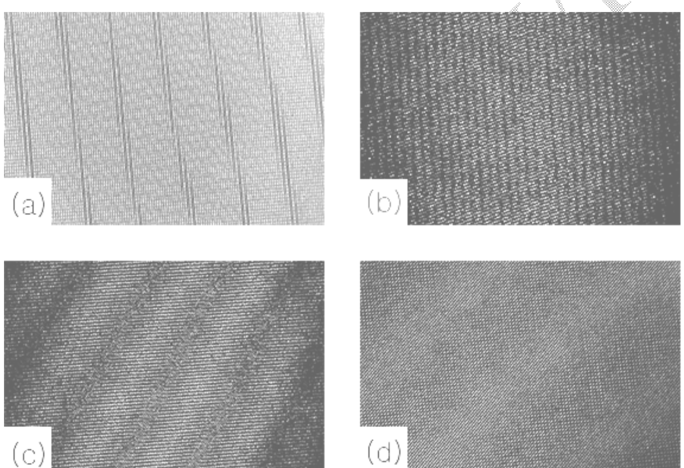

Fig. 6. Illustration of a variety of moiré fringes. (Photographs ordered be tangents: 0, 1/3, 2/3, 1.)The full set of the experimental data is graphically shown in Fig. 7 below.
(a) φ= 0°, σ= 1.5, ρ = 0.72; (b) φ= 18°, σ= 0.33, ρ = 0.55;
(c) φ= 33°, σ= 0.67, ρ = 0.55; (d) φ= 45°, σ= 0.5, ρ = 0.72. Reproduced with permission from [19]. © The Optical Society.

The angle between the static grid and the barrier plate was changed from 0 to 90°. We estimated the period of the moiré patterns and recorded the local maxima of the period as the moiré angles. In this experiment, we had a variety of combinations of cells and plates; the gratings with 13 different aspect ratio values were used.

We conducted two experiments: with cells with an arbitrary aspect ratio and with square cells (with an aspect ratio of 1).

3.2.1.Clustering of Experimental Data(Arbitrary Aspect Ratio)in Parameter Space

In experiments with arbitrary aspect ratios, we observed that the moiré angle φ gradually changes when the aspect ratio changes.

In the overall picture of all experiments in the parameter space (experimental data drawn in the graph tan(φ) vs. σ), the abscissas and ordinates of the experimental points were distributed more or less uniformly (especially, abscissas between 0.8 and 1.5 and ordinates between 0.17 and 1.6), see Fig. 7. However, this overall picture does not show a uniform distribution of the experimental points across the entire area of the parameter space.

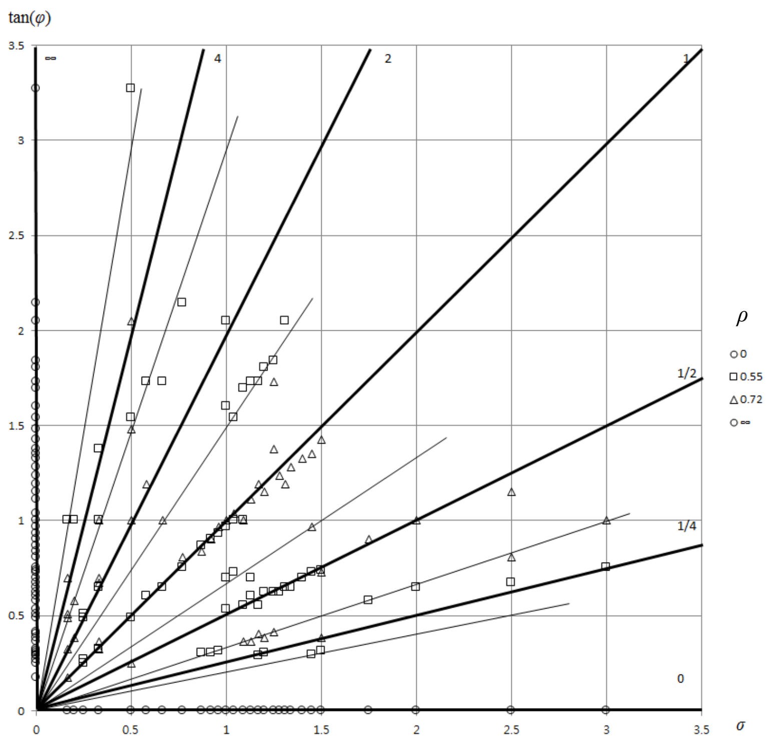

Fig. 7. Full set of experimental data: the tangent of the moiré angle φ as a function of aspect ratio σ. (Square and triangle markers show $\rho = 0.55$ and 0.72). Clustering of experimental data along rays. Constants of proportionality are indicated near somerays. Reproduced with permission from [19]. © The Optical Society.

A careful look at Fig. 7 can uncover that the experimental data are concentrated (clustered) within a closeneighborhood of the rays with the rational slope angles, and mainly, there are at least three recognizable straight lines comprised from the experimental points at the moiré angles φ: 0, 45°, and 90°. The vast majority of the experimental data falls within these neighborhoods. We refer to this phenomenonas the 'clusterization along the rays', which describes the concentration of experimental data within narrow boundaries around the rays with the rational slope angles. Particular values of ρ do not affect clustering.

The normalized room-mean square (NRMS) deviation between the experimental points and the corresponding rays with the rational tangents is 1.7%. Along the rays, the tangent of the moiré angle $\varphi$is generally proportional to the aspect ratio. This fact virtually excludes the existence of a preferable aspect ratio to minimize the moiré effect. Nevertheless, one can utilize the areas between the rays in the parameter space for the minimization.

3.2.2. Clustering of Experimental Data2

The experimental data with the rational abscissas and small k, $l$are arranged differently than the general picture described above.The vertical cross-sections of Fig. 7 graphically represent a subset with specific k and l at fixed values of σ.

While the primary feature described above (ray clusterization) is kept, another trend was identified in the subset of the experimental data. To verify that, eight rational aspect ratios with k, $l \leq 4$ were selected from the dataset (namely, 1/4, 1/3, 1/2, 2/3, 1, 3/2, 2, and 3). The shape of such cells includes the square,and the squareis divided into several equal parts. In each test, several (from 1 to 5) moiré angles were observed, so the total number of angles in experiments with these ratios is 26 (except for the "permanent" angles 0 and 90°). The number of the observed moiré angles φ is several times higher than the number of aspect ratios; therefore, one may expect a wide variety of the moiré angles. However, while the abscissas are located more or less uniformly, the most ordinates are concentrated around a few values. See Fig. 8, where some horizontal lines are drawn, where the experimental data are concentrated.One can observe clusteringalong the horizontal linesinFig. 8, where the data values are concentrated in several groups with practically empty areas between them.

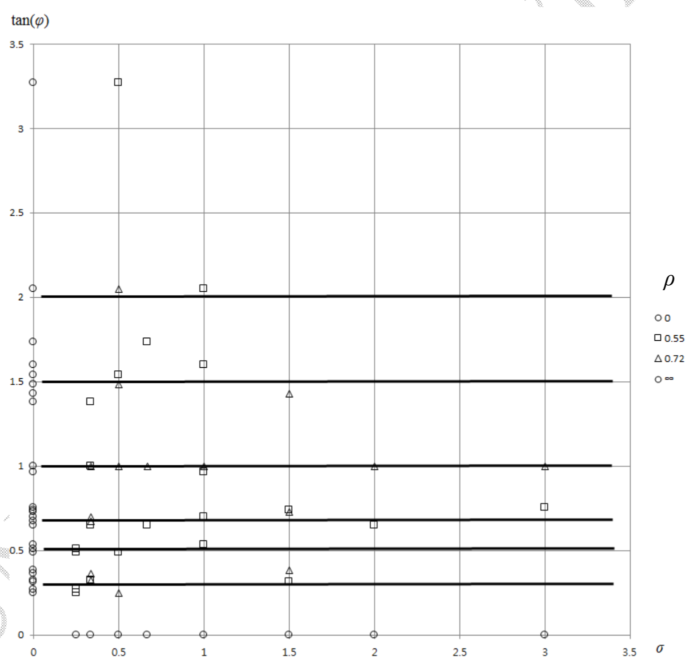

Fig. 8. Discrete moiré angles φ (experimental).Clusteringof the experimental data with "small rational" aspect ratios. Reproduced with permission from [19]. © The Optical Society.

In this subset,the ordinates of the experimental points can bearranged into ten groups with the NRMS deviation from the center of each group less than 5%; the centers of these groups of localization are 0.26, 0.32, 0.37, 0.51, 0.68, 0.74, 0.98, 1.38, 1.48, and 1.67. These ten listed values, together with the values 2 and 3 (which cannot be characterized statistically because of a very few occurrences in this experiment) are very close to the following rational numbers: 1/4, 1/3, 3/8, 1/2, 2/3, 3/4, 1, 11/8, 3/2, 5/3, 2, 3.

This subset of experimental data confirms the trend for “small rational” abscissas to be clustered around “small rational” ordinates. A few moiré angles were observed with the aspect ratios with small k and $l$in the expression of the rational numbers for their tangents.

This feature can be treated as the discrete moiré angles in grids with square cells divided into parts, as in typical LCD devices. It has the potential to affectthe display technology. It means that the most angles of the noticeable moiré effect in the square cells divided vertically in 2 or 3 equal parts are the same in the square cells. This finding could inspire new applications and innovations in the field.

To summarize this subsection, we observed general ray clustering and horizontal clustering. Most (75%) of the moiré angles φ observed in this subset of barrier experimentwith $k, l \leq 4$ are the rational angles defined by Eq. (1).

3.3.Experimental Moiré Angles and Clustering in LCD Displays (Square Pixels)

The clusterization of the moiré angles $\varphi$with small k, l(see the previous Section) was experimentally observed in LCD panels (square pixels with σ = 1) for all combinations of panels (4 devices) with barrier plates of 3 types. Examples of the moirépatterns in LCD panels are shown in Fig. 9.All observed moiré angles are listed in Table 3. In the graph tan(φ) vs. σ (as Fig. 7), all these data lie along the vertical lineσ= 1.

Table 3. Moiré angles observed in LCD panels combined with barrier plates.

LCD panel	Barrier pitch, mm	Size ratio ρ	Measured moiré anglesφ				
A	0.44	1.62	-1.1°	17.8°	26°	33.5°	44.6°
A	0.57	2.12	-1.2	184°	26.2°	33.2°	43.9
B	0.44	2.05	1.6°		28.6°		47.4°
B	0.57	2.67	0.03°		27.8°		46.1°
C	0.44	2.15	-1.1°	17.9°	26.9°	34°	44°
C	0.57	2.80	-1.2°	18.4°	26.6°	32.7°	44.4°
D	0.44	2.30	0.3°				
D	0.57	3.00	0.6°		27.1°		45.9°
B	0.45	2.11	0.1°		25.5°		46°
C	0.45	2.21	-0.1°	19°	26.8°	34.6°	45.4°
A	0.45	1.67	0.7°	18.4°	26.9°		45.0°

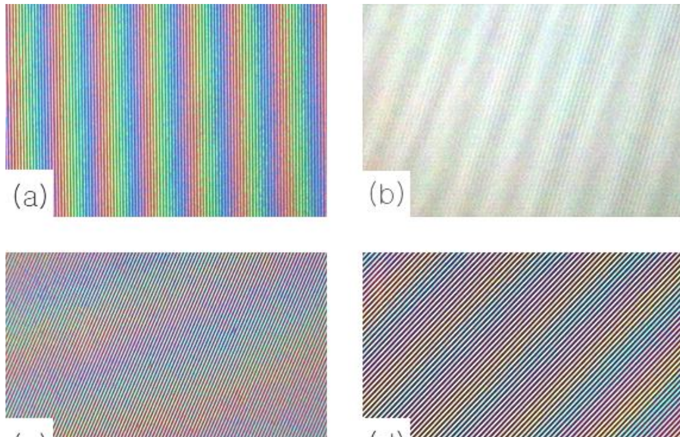

Fig. 9. Illustration of moiré fringes in LCD displays (σ= 1).
(a) φ= 0°, device D,ρ = 3.00; (b) φ= 18°, device C,ρ = 2.80; (c) φ= 33°, device B,ρ = 2.67; (d) φ= 45°, device C,ρ = 2.80;
The corresponding set of the experimental data is given in Table 3.Reproduced with permission from [19]. © The Optical Society.

The experiment with the rational aspect ratios in printed samples (Sec. 3.2.2, small k, l) has revealed a significant similarity with the moiré angles φ in the square LCD pixel cells. These angles are remarkably close to the angles with the rational tangents 0, 1/3, ½, 2/3, and 1, with an NRMS deviation of only 2.5%. This is of great significance and sheds new light on the understanding of the moiré effect.

3.4.Summary of Barrier Experiments

Among all moiré angles φ in the rational cells with $1 \leq k, l \leq 6$, the moiré effect occurred more frequently at certain particular angles. Based on the count of cases in the experiment, we can classify the moiré angles φ in "rare" and "frequent" categories as follows. If the moiré effect was observed only once, it is a "rare" angle; otherwise (i.e., if it happened twice and more, or up to 12 times in the experiment), it is a "frequent" angle. There are few cases at many "rare" angles, but many moiré cases are at a few "frequent" angles. These are distributed as follows: 12% of "rare" cases (8 angles, 8 cases), 79% of "frequent" angles (8 angles, 53 cases), and 9% remaining (3 angles, 6 cases) which do not show any specific behavior and there are not many angles and not many cases. The tangents of "rare" angles are as follows: 1/6, 3/10, 3/8, 2/5, 3/5, 5/3, 9/4, 3; the tangents of "frequent" angles are 0, 1, 1/2, 2/3, 3/4, 3/2, 2, ∞; the intermediate tangents are 1/4, 1/3, 4/3.

In other words, the moiré effect at the "rare" angles was observed only in very few cases; the moiré effect mostly does not happen here. The moiré effect almost always occurred at the "frequent" angles. However, the moiré effect may sometimes not happen at the intermediate angles.

Furthermore, most (79%) of the "rare" angles are the rational angles Eq. (1) with one of m, $n \geq 4$. Most (88%) of the "frequent" angles are the angles φ_{mn} with both m, $n \leq 3$. The intermediate angles haveone of m, $n$is equal to 3 or 4.

This classificationcan give a key to select preferable angles to minimize the moiré effect in displays. Correspondingly, the rational angles$\varphi_{mn}$with m, n> 4 are suitable candidates for moiré-less angles where the moiré effect would be exceptional. Therefore, it can be suggested that under some additional conditions (assumable, the size ratio) such rational angles can be moiré-free angles in grids with rational aspect ratios. For instance, the tangents of the rational angles $4<m$, $n<7$ are asfollows: 1/5, 2/5, 3/5, 4/5, 1/6, 5/6 (the reducible fractionsm/n are not included in the list). In practical minimization, the listed angles shouldbe tried first.

The experimental data show that within the angular range0 – 90° (between the axis of the plate and the vertical axis), the moiré effect has maxima at approximately 25 angles total, but typically, there are 3 to 8 moiré angles for a particular σ. In the rational cells (either LCD or printed), the detected moiré angles are the rational angles by Eq. (1). The experimentally observed rational angles have$m$, $n \leq 11$. However,the numbers are considerably smaller, i.e., m, $n \leq 5$for the great majority of the moiré angles (more than 70%),

3.5. Experimental Moiré Angles and Clustering in Lenticular Displays

Examples of the observed moiré patterns in lenticular displays are shown in Fig. 10. The experimental equipment is described in Sec. 3.1.

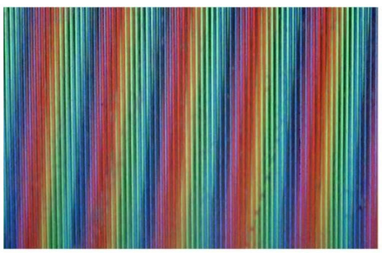

(a)

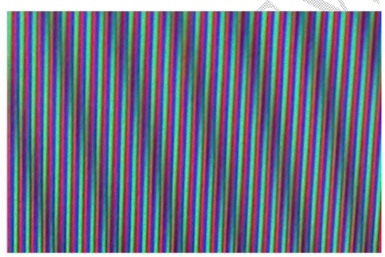

(b)

Fig. 10. Examples of moiré patterns in LCD displays with lenticular plates. The period of pixels is 0.204 mm in (a) and 0.266 mm in (b); the plates 50 lpi and 40 lpi were attached (periods 0.508 mm and 0.635 mm, resp.) Reproduced with permission from [21]. © The Optical Society.

The clusterizationof moiré angles φ is confirmed in the experiment with square pixels (σ = 1). We performed this experiment with several LCD devices and lenticular plates (instead of barrier plates); 5 LCD panels with square pixels and 4 lenticular plates.

As in the barrier case, the lenticular experiment confirms the rational angles in LCD displays. We observed visible moiré fringes across the angular range 0°- 45° in the experiment with the lenticular plates only at a few fixed angles.The experimental data is given in Table 4. The NRMS deviation between the tangents of the observed moiré angles and the corresponding rational numbers of 0, 1/3, ½, 2/3, and 1 is 0.5%. The graphical representation of this experiment in a graph similar toFig. 7is a vertical line. This experiment is in accordance with the barrier experiment.

Table 4. Observed moiré angles φ in LCD panels combined with lenticular plates.

LCD panel	Lenticular plate (lpi)	Size ratio ρ	Measured moiré angles				
E	40	2.5	0°	19°	27°	35.3°	46°
A	25	3.76		19°	26°	33°	
E	12	3.79	0°	18.4°	27.3°	34.4°	45°
F	25	3.82		19°	27.5°	34°	
C	25	4.98		18.4°	26.9°	33.7°	
D	25	5.33	0.2°		27.1°		44.3°
A	15	6.27		18°	26.9°		
F	15	6.37			26.5°		

C	15	8.3		19.5°	26.5°	33°	
D	15	8.89	0°				45°

Independent researchers have observed previously observed a similar behavior of moiré patterns. For example, the research paper [23] describes the moiré effect in the 22" 3D display with the aspect ratio $\sigma \neq 1$. Thatdisplay device has a non-typical layout of pixels: square pixels are divided into two halves. (Such a layout does not affect the visual image on this screen because both halves work synchronously.) However, this affects the appearance of the moiré effect, since the vertical period becomes twice as short. In that display, $\sigma = 2$, $\rho = 7.90$, and the moiré “patterns are vivid and more distinct when the slant angle is 0, 18°, 19°, 34°, 35°”, as reported in [23]. Note that the items on this list are close to the angles with the rational tangents 0, 1/3, and 2/3. This fact can be considered an independent experimental confirmation of the discrete moiré angles φ_{mn} in displays with divided square pixels.

It is also interesting to mention here that the widely used angle 30° between the screens in color printing [1], [24] is very close to the angle (atan3/5) found in the current Chapter.

4. Probability of the Moiré Effect

The classification of the angles (“rare” and “often”) together with their clusterization in the parameter space gives a rise to another approach.

Using the experimental data, we can estimate the probability of the moiré effect based on the number of observed moiré cases in all particular testsfor all screens combined with different barrier plates, as in [13]. When we observe the moiré effect in various devices, the number of successful attempts (with the moiré effect) is counted for each angle without regard to σ. The relative count of the successful cases means the probability. According to [21], the moiré patterns were not observed at the irrational angles experimentally; in such case, the probability at the mentioned angles is zero.

4.1. Experimental Probability

Figure11 shows the resulting function for barrier displays. The vertical bars show the probability. This is an experimental probability of the moiré effect observed in experiments, which shows an expectation of the moiré effectas a function of the angle. The function models the maxima of the moiré period only, and therefore the value of the function between the peaks is zero.

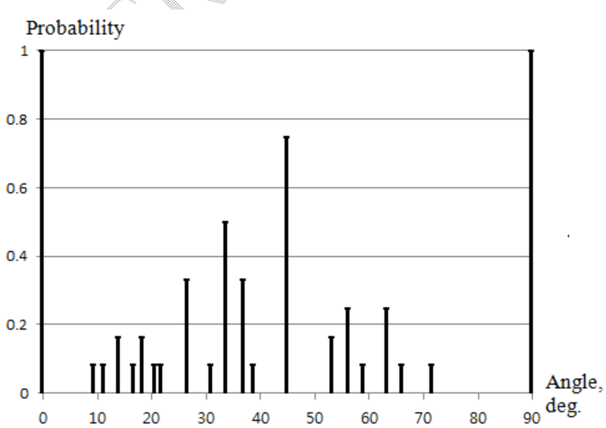

Fig. 11. Experimental moiré probability function for autostereoscopic barrier displays. Reproduced with permission from [21]. © The Optical Society.

The lenticular probability function builtprecisely as the barrier probability function is shown in Fig. 12.

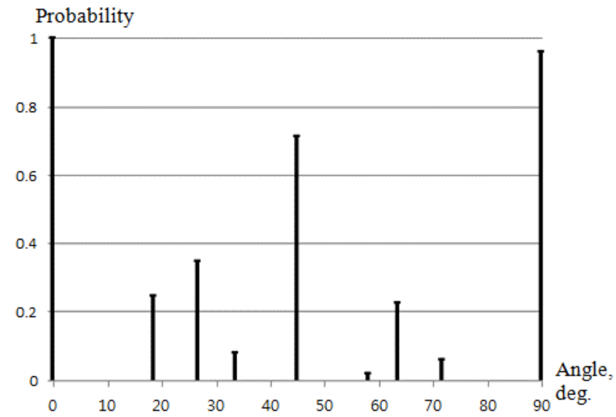

Fig. 12. Experimental probability of the moiré effect in LCD displays with lenticular plates. Reproduced with permission from [21]. © The Optical Society.

The probability of the moiré effect for the lenticular displays is similar to the function of the barrier displays, despite the different number of moiré angles. The locations and heights of the peaks of both functions in Figs. 11 and 12 nearly coincide.

Therefore, a common (composite) probability function for both barrier and lenticular displays can be built based on the two experimental data sets. It merges the weighted barrier and lenticular functions, as shown in Fig. 13.

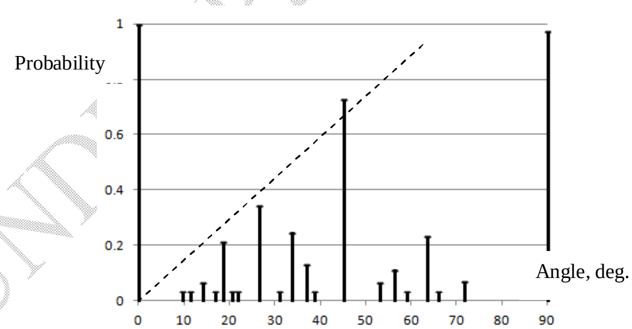

Fig. 13. Common experimental probability. Adapted with permission from [21]. © The Optical Society.

4.2. Experimental Probability vs. Theory

The experimental and theoretical functions presented in Sections 2 and 3 appear similar. In particular, almost all peaks in Fig. 13 have an analogue in Fig. 3. The positions of the corresponding peaks of both functions practically coincide; their heights are also close.

The similarity of functions can be estimated based on the distance between them. In order to make a comparison, we define the distance between two functions, F_1 and F_2as the root-mean-square (RMS) deviation,

$$\Delta_{RMS}\left(F_1, F_2\right) = \sqrt{\frac{\sum_i \left(F_1(x_i) - F_2(x_i)\right)^2}{N}} \quad (4)$$

where $F_1$and $F_2$are the functions defined in points x_i, N is the number of points of comparison of the functions.

As defined above, the calculated distance between the functions of the experimental probability and the spacing (i.e., between the measured probability and the theoretical spacing of nodes) for the barrier displays is 11.8%. The experimental probability of lenticular displays can also be compared to the theory; here, the distance between the experimental and theoretical functions is 15.5%. Similarly, the distance between the composed experimental probability function and the theory is 14.2%.

All three distances are less than 15%. Therefore, the spacing function defined by Eq. (2) can be considered as a reasonable mathematical approximation for the experimental probability of the moiré effect.

5. Related Functions

Except for the spacing function, there are other similar functions related to the probability directly or indirectly.

5.1. Thomae's Function

TheThomae's functioncharacterizes the rational numbers, i.e., the tangents of slant angles. The Thomae's function is defined as follows [25] (see also Fig. 14),

$$T(x) = \begin{cases} c & \text{for rational angles } (x = m/n) \\ d & \text{for non-rational angles} \end{cases} \quad (5)$$

where c and d are real numbers (usually, $c = 1$, $d = 0$).Sometimes, this function is called the modified Dirichlet function.

The locations of peaks of Thomae's function (after certain renormalization of its abscissas, because the Thomae's function is defined on the segment between 0 and 1 while the spacing function for the angles between 0° and 90°) coincide with the peaks of the spacing function, although the heights are slightly different.

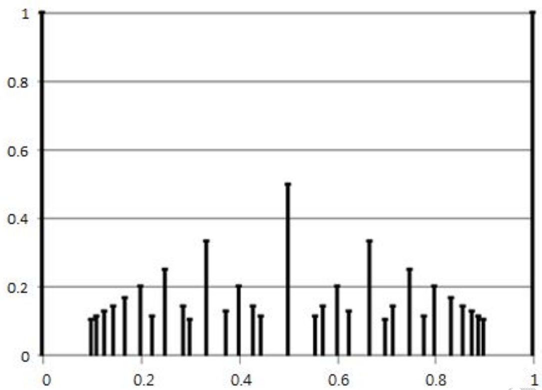

Fig. 14. Thomae's function for $n \leq 10$. Reprinted with permission from [21]. © The Optical Society.

The locations of peaks of Thomae's function coincide with the peaks of the spacing function, although the heights are slightly different. Note that comparing these functions needs the renormalization of abscissas.

The distance between the experimental probability and Thomae's function can be found based on RMS by Eq. (4). For the barrier case, it is 12.5%; for the lenticular, 18.7%; and for the composed function, 15.2%. These percentage values are very close to the percentage differences of the spacing function (the difference between them is less than 3%). However, based on such negligible difference, the preferable mathematicalfunction for the analytical estimation of the moiré probability cannot be unambiguouslychosen because the distance between the functions is larger than 8%.

The relationship between the spacing and Thomae's functions defined by Eqs. (2) and (5) can be analytically derived as follows. The ratio of these functions to the rational angles is

$$\frac{T(x)}{D(x)} = \sqrt{1+\left(\frac{m}{n}\right)^2} \tag{6}$$

For $m/n \leq 1$, the infinite series for $(m/n)^2$ can replace the square root in Eq. (6),

$$\frac{T(x)}{D(x)} = 1+\frac{1}{2}\left(\frac{m}{n}\right)^2 - \frac{1}{8}\left(\frac{m}{n}\right)^4 + \frac{1}{16}\left(\frac{m}{n}\right)^6 - \ldots \tag{7}$$

When $m/n < 1/2$, the second term in Eq. (7) is approximately one order less than the first and, therefore, can be neglected; however, when the ratio m/n is increased, the two terms become comparable. Therefore, for smaller proportions m/n (less than 1/2, i.e., the angles < 27°), the two functions nearly coincide, but for larger ratios (the angles > 27°), the functions becomesignificantly different.

5.2. QualityFunction

Another function, the quality function [26], looks very similar to Thomae's function (and therefore to the experimental probability of the moiré effect, too). In Fig. 15,the maxima of thequality function are shown in relative coordinates across one period of the function in the projective space; the function varies from 0 (lowest quality) to 1 (the highest quality).

The physical nature of the quality function is entirely different; this function estimates the quality of a visual image in an autostereoscopic display in the projective space. Despite that, the locations and the heights of peaks of the function [26] appear to be very similar to those of the spacing function by Eq. (2). Consequently, it is similar to Thomae's function and the experimental probability of the moiré effect.

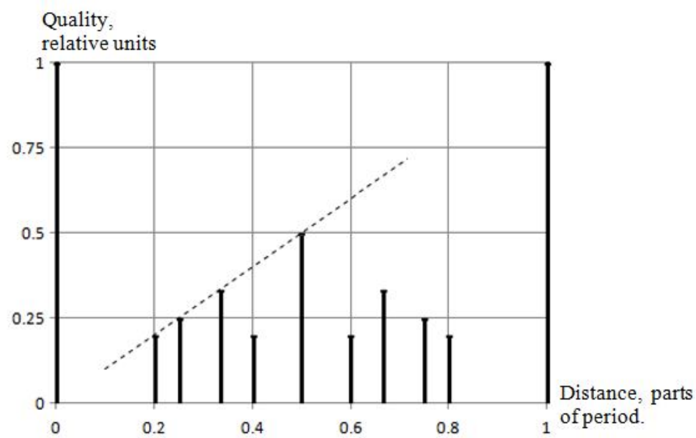

Fig. 15. The maxima of quality function for autostereoscopic displays in the relative coordinates across one period. Reprinted with permission from [21]. © The Optical Society.

5.3. Envelope Line of Related Functions

Also, it is not uninteresting to find that the "envelope" line passing near the tops of the peaks can be recognized in all mentioned functions: probability, spacing, Thomae's, and quality. This is the dashed line from the origin (0, 0) to the point (1, 1) in Fig. 15 and the equivalent line in Fig. 13. Furthermore, In Figs. 3 and 14, one can easily recognize the similar envelope lines.

The relations between the mathematical and experimental functions require additional investigation, as well as the physical meaning of the envelope line.

6. Discussion

Despite the similar probability functions, there are some physical differences between the 3D displays of different types. Namely, in the barrier displays, neither the distance from the LCD to the barrier plate nor from the display to the observer affects the observed moiré angles. Notably, the moiré patterns in the barrier displays appear at the same angles without respect to the mentioned distances.

However, in the case of the LCD with the lenticular plate, acertain preferred distanceprovides the most substantial moiré effect. Similarly, the distance to the observer strongly affects the visibility of the moiré patterns. Therefore, the moiré angles in lenticular displays may depend on the mentioned distances. To illustrate, the distance to the plate is near the focal distance of the lenticules according to the well-known thin lens equation [27]. Otherwise, there are no visible moiré patterns in the lenticular display (and such a "display" with the wrong distance will not support stereoscopic imaging at all). In experiments presented in the current Chapter (both lenticular and barrier cases), the distance to the camera was 50 cm.

The research paper [28] confirms the less visible moiré pattern at the slant angle of 23.96°. The papers [29], [30] also use Thomae's function in the analysis of the prime numbers and in the spectral analysis. The paper [31] describes the moiré effect as "geometrical], nonlinear phenomenon obtained by the superposition of two repetitive microscopic structures (two grids) of neighboring spatial frequencies, which show small deviations either in the structure itself, in their positions". The paper [32] demonstrates the difference between the rational and non-rational angles for the moiré effect in LED displays.

One can use the statistics for the minimization of the moiré effect by angle. The statistical approach shows that, among the rational angles, the probability of the moiré effect depends on the integer numbers m, n, defined in Eq. (1). In the nonsinusoidal case, the moiré patterns caused by higher harmonics were observed in digital displays in the close neighbourhood of the rational angles with $m, n \leq 5$ [19], [33]. Then, given integers m and n, the spacing function Eq. (2) estimates the probability; between the rational angles, the probability is theoretically zero. Practically, it is somewhere between $(m^2 + n^2)^{-1/2}$ and zero with small m, n (say, less than 5).

Figures5, 6, 9, 10are given to illustrate the variety of the observed moiré fringes, while the experimental results are presented in Figs. 7, 8, 11, 12, and in Tables 3, 4.

Based on experimental measurements and statistics, one can find two options to minimize the moiré effect by the angle: either to use a nonrational angle (where the probability is theoretically zero) or to select a rational angle with a low probability of the moiré effect using the probability function, as it was suggested in [21]. One should keep in mind that the width of the moiré peak is finite and does not equal zero, even for the narrowest peaks. This can be seen in the experimental graph given in Fig. 1.

The formula for the width of the bell-shaped curve of the moiré amplitude is obtained in [12]. The formula shows that "when the ratio of the periods of the gratings is equal to 1, the width is zero. This means that for the exactly n-fold (matching) periods, the moiré period behaves as the delta function; for other (larger or smaller) ρ, it widens." (The quote from [34].) This feature was practically used in the display device developed by one author of [12], which display "had the exact match of periods (the ratio ρ = 4.0), and thus the width of the period function was very narrow. As a result, in that display, the moiré patterns were absent even at the small twist angles (about 6°), despite that at the zero angle, the probability (and, correspondingly, the visibility) of the moiré patterns is highest." (The quote from [34].)

The experimental results presented in the current Chapter are based on the visual estimation of the moiré patterns; this gives a binary answer about the absence or presence of the moiré patterns based on the patterns whose amplitude exceeds a certain threshold. For future development, the semi-automatic measurement of the moiré waves is not impossible [35], as is using perfect instruments by ELDIM, in particular the tool [36], to measure the moiré effect in 3D displays.

7. Conclusion

We experimentally measured the angles of the moiré effect. The experiments were conducted to find some possible preferable values of the geometric parameters. We scanned the angular range 0 - 90°for the moiré effect and measured the angles of the visible moiré patterns. The overall range of parameters covered in the experiments is as follows: the period ratio ρ from 0.18 to 8.89, the aspect ratio σ from 1/6 to 3. Such parameters are typical for autostereoscopic multiview and integral imaging displays.

We found that the moiré angles are clustered in the parameter space. Clustering was observed along inclined lines and horizontal lines. In cells with the rational aspect ratioand small integer numbers k, l (as in LCD panels), the moiré patterns appeared at a few discrete angles withboth barrier and lenticular plates. We did not identify a preferable aspect ratio for minimizing the moiré effect.

The probability of the moiré effect as a function of the angle was based on the experimental data. Combining the probability functions for lenticular and barrier displays, we created a common composite function. A mathematical description of the probability of the moiré effect in visual displays with rational cells (the spacing function) was proposed. This function is similar to the known Thomae's function and can be used to estimate the probability.

The results can be used for the minimization of the moiré effect. There can be two options for minimizing the moiré effectin terms of probability: use non-rational angles (where the moiré patterns have not been observed experimentally and the probability is zero) or choose a rational angle with a low probability of the moiré effect. It is important to remember that the width of moiré peaks is finite and does not equal zero. The mentioned options are essential for improvingthe image quality in the autostereoscopic 3D displays, where the moiré effect may significantly reduce the visual contrast of the image.

References and links

1. I. Amidror, *The Theory of the Moiré Phenomenon,*vol. 1, Springer (2009).
2. K. Patorski and M Kujawinska, *Handbook of the Moiré Fringe Technique,*Elsevier Science Publisher (1993).
3. K. Creath and J. C. Wyant, “Moiré and fringe projection techniques,” in *Optical Shop Testing*, Second Edition, Chap. 16, John Wiley & Sons (1995).
4. J. Hong, Y. Kim, H. J. Choi, J. Hahn, J. H. Park, H. Kim, S. W. Min, N. Chen, and B. Lee, “Three-dimensional display technologies of recent interest: principles, status, and issues,” *Appl. Opt.***50**(34), H87-H115 (2011).
5. B. Lee, S.-G. Park, K. Hong, and J. Hong, *Design and Implementation of Autostereoscopic Displays*, Bellingham, Washington: SPIE (2016).
6. A. Stern and B. Javidi, “Three-dimensional image sensing, visualization, and processing using integral imaging,” *Proc. IEEE***94**, 591-607 (2006).
7. R. Martinez-Cuenca, G. Saavedra, M. Martinez-Corral, andB. Javidi,“Progressin3-Dmultiperspective display by integral imaging,”*Proc. IEEE***97**, 1067-1077 (2009).
8. L. Kong, G. Jin, T. Wang, “Analysis of moiré minimization in autostereoscopic parallax displays,” *Opt. Express***21**, 26086 (2013).
9. V. Saveljev, “Orientations and branches of moiré waves in three-dimensional displays,” *J. Korean Phys. Soc.***57**(6), 1392-1396 (2010).
10. V. Saveljev, J.-Y. Son, B. Javidi, K.-T. Kim, S.-S. Kim, and D.-S. Kim, “Moiréminimization condition in three-dimensional image displays,” J.Displ. Technol. **1**(2), 347-353 (2005).
11. V. Saveljev and S.-K. Kim, “Moiré period as function of angle for moiré minimization in autostereoscopic 3D displays,” in *Proceedings ofOptical Society of Korea Summer Meeting*, p. W1G-VII4, Gyeongju, Korea (2015).
12. V. Saveljev and S.-K. Kim, “Amplitude, period and orientation of the moiré patterns in barrier 3D displays,” *J. Inf. Disp*. **19**(2), 81-90 (2018).
13. V. Saveljev and S.-K. Kim, “Estimation of Probability of the Moiré Effect,” in Proceedings of Collaborative Conference on 3D and Materials Research (CC3DMR), pp. 397-398, Busan, Korea (2015).
14. V. Saveljev, *The Geometry of the Moiré Effect in One, Two, and Three Dimensions*, Cambridge Scholars Publishing (2022).
15. R. P. Williams, D. H. Davies, and G. Harburn, “On randomization techniques for the suppression of unwanted moiré patterns in images generated by a scanning system with a periodic amplitude defect,” *Optica Acta***33**(10), 1311-1319 (1986).
16. P. Hopstone, A. Katz, and J. Politch, “Infrastructure of time-averaged projection moiré fringes in vibration analysis,” *Appl. Opt.* **28**(24), 5305-5311 (1989).
17. L. Meng, R.Wu, L. Zhang, L. Li, S. Du, Y. Wang, and H.-J. Gao, “Multi-oriented moiré superstructures of graphene on Ir(111): experimental observations and theoretical models,” *J. Phys.: Condens. Matte*r **24**, 314214 (2012).
18. C. Li, Z. Liu, H. Xie, and D. Wua, “Statistics-based electron moiré technique: a novel method applied to the characterization of mesoporous structures,” *Nanoscale***6**, 13409-13415 (2014).
19. V. Saveljev and S.-K. Kim, “Experimental observation of moiré angles in parallax barrier 3D displays,” *Opt. Express***22**(14), 17147-17157 (2014).

20. V. Saveljev and S.-K. Kim, "Experimental probability of moiré effect in autostereoscopic displays with lenticular plate," in *Proceedings of22th Conference on Optoelectronics and Optical Communications* (COOC), pp. 263-264, Busan, Korea (2015).
21. V. Saveljev and S.-K. Kim, "Probability of the moiré effect in barrier and lenticular autostereoscopic 3D displays," *Opt. Express***23**, 25597-25607 (2015).
22. D. Zwillinger, *CRC Standard Mathematical Tables and Formulae*, CRC Press, Chap. 4.4 (2002).
23. Y.Kim, G.Park, J.-H.Jung, J.Kim, and B.Lee, "Color moiré pattern simulation and analysis in three-dimensional integral imaging for finding the moiré-reduced tilted angle of a lens array," *Appl. Opt.***48**, 2178-2187 (2009).
24. S.S. Deshpande, "Screen angle combinations and effect on print quality parameters," *Int. J. Adv. Eng. Technol.***II**(IV), 480-482, (2011).
25. S. Abbott, *Understanding Analysis* (Springer, 2001), Chap. 4.1.
26. V. Saveljev, J.-Y. Son, S.-B. Woo, M.-C. Park, D.-S. Lee, and K.-D. Kwack, "Quality estimation for visual image in autostereoscopic 3D display," *Proc. SPIE***7329**, 73290O (2009).
27. F.A. Jenkins and H. E. White, *Fundamentals of Optics* (4th Edition). Singapore, McGraw-Hill Education, p. 140 (1981).
28. Z. Zhuang, P. Surman, L. Zhang, R. Rawat, S. Wang, Y. Zheng, and X.W. Sun, "Moiré-reduction method for slanted-lenticular-based quasi-three-dimensional displays,"*Opt.Commun.***381**(15), pp. 314-322 (2016).
29. T.C. Petersen, M. Ceko, I.D. Svalbe, M.J. Morgan, A.I. Bishop, and D.M. Paganin, "Simple wave-optical superpositions as prime number sieves," preprint *arXiv*:1812.04203v2 [physics.optics], 12 Mar 2019
30. X.-S. Xia, X.-L. Cai, Z.-H. Li, C.-C Shen, W.-F Liu, Y.-Q. Jin, F.-T. Sang, and J.-W. Guo, "Algorithm for broadband Brillouin spectra analysis based on Thomae's function,"*Acta PhotonicaSinica***49**(6), 0630003 (2020).
31. M. Rahima and M. Said, "Detection of the micro defects on the transparent optical materials by the topographic moiré," *Math. Model. Eng. Probl.***3**(4), pp. 198-201 (2016).
32. K.Lin, N. Liao, D. Zhao, S.Dong, and Y. Li, "Analysis of moiré minimization in color LED flat-panel display,"*Proc. SPIE***9618**, pp. 96180K, (2015).
33. V. Saveljev and S.-K. Kim, . "Estimation of contrast of moiré patterns in 3D displays," Proc. *14^{th} International Meeting on Information Display* (IMID), Daegu, Korea, p. 417 (2014).
34. V.Saveljev, W. Han, H. Lee, J. Kim, and J. Kim, "Moiré effect in double-layered coaxial cylinders," Appl. Optics 59(18), 5596-5607 (2020).
35. V. Saveljev and S.-K. Kim, "Simulation and measurement of moiré patterns at finite distance," *Opt. Express***20**(3), 2163–2177 (2012).
36. P. Boher, T. Leroux, T. Bignon, and V. Collomb-Patton, "Full optical characterization of auto-stereoscopic 3D displays using local viewing angle and imaging measurements," *Proc. SPIE***8288**, 82880S (2012).